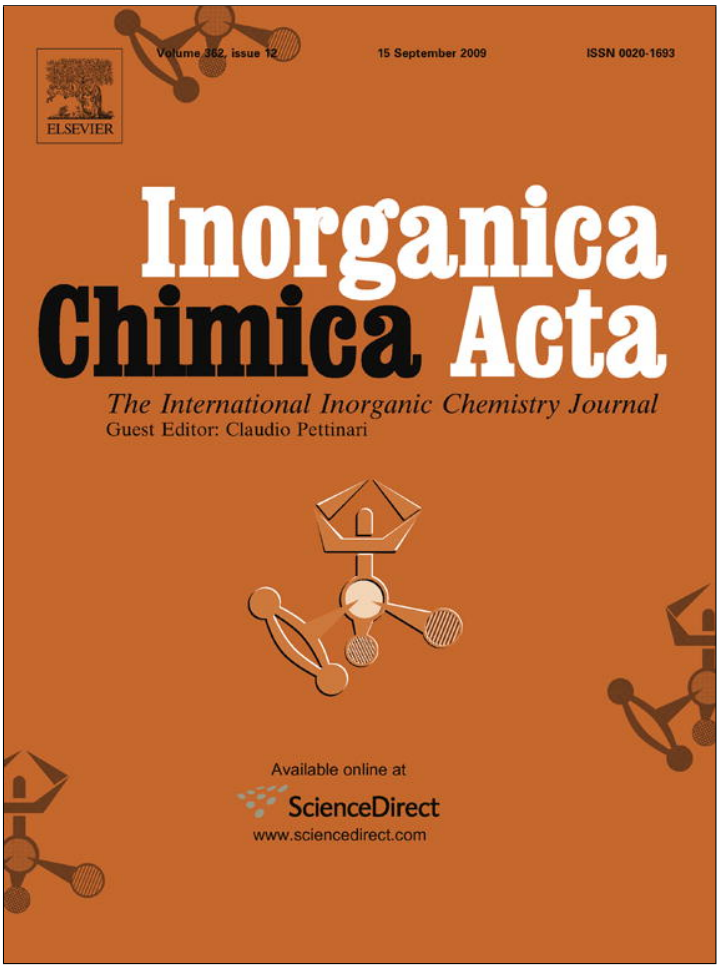

Inorganica Chimica Acta 362 (2009) 4449–4460

Contents lists available at ScienceDirect

Inorganica Chimica Acta

journal homepage: www.elsevier.com/locate/ica

# Synthesis and spectroscopic investigations of four-coordinate nickel complexes supported by a strongly donating scorpionate ligand

Ismael Nieto [a], Ranko P. Bontchev [b], Andrew Ozarowski [c], Dmitry Smirnov [c], J. Krzystek [c], Joshua Telser [d], Jeremy M. Smith [a,*]

[a] Department of Chemistry and Biochemistry, New Mexico State University, MSC 3C, P.O. Box 30001, Las Cruces, NM 88003-8001, USA
[b] Cabot Corporation, 5401 Venice Ave. N.E., Albuquerque, NM 87113, USA
[c] National High Magnetic Field Laboratory, Florida State University, 1800 E. Paul Dirac Dr., Tallahassee, FL 32310, USA
[d] Department of Biological, Chemical and Physical Sciences, Roosevelt University, 430 S. Michigan Ave., Chicago, IL 60605-1394, USA

ARTICLE INFO

*Article history:*
Received 22 January 2009
Received in revised form 30 April 2009
Accepted 7 May 2009
Available online 18 May 2009

Dedicated to Swiatoslaw Trofimenko.

*Keywords:*
Scorpionate ligands
Nickel complexes
Spectroscopy

ABSTRACT

Two four-coordinate nickel complexes, HB($^t$BuIm)$_3$NiBr and HB($^t$BuIm)$_3$NiNO, were prepared by reaction of a bulky tris(carbene)borate ligand with $NiBr_2(PPh_3)_2$ and $NiBr(NO)(PPh_3)_2$, respectively, and structurally and spectroscopically characterized. In addition to standard techniques, high-frequency and -field electron paramagnetic resonance (HFEPR) was employed to understand the spin triplet ($S = 1$) ground state of the bromo complex. HFEPR, combined with electronic absorption spectroscopy allows comparison of this novel complex with other paramagnetic four-coordinate Ni(II) species. The tris(carbene)borate ligand is a stronger σ-donor than corresponding tris(pyrazolyl)borates (traditional "scorpionate" ligands). The tris(carbene)borate ligand may also act as a π-acceptor, in contrast to tris(pyrazolyl)borates, which show relatively little π-bonding interactions. The influence of tris(carbene)borate substituents on the donor strength of the ligand have been elucidated from IR spectroscopic investigations of $\{NiNO\}^{10}$ derivatives. HFEPR spectra of HB($^t$BuIm)$_3$NiBr exhibit hyperfine coupling from Br, which indicates the strong electronic interaction between Ni(II) and this halide ligand, consistent with studies on tris(pyrazolyl)borate Ni(II) complexes.



## 1. Introduction

From their genesis in the 1960s, scorpionate ligands developed by the late Swiatoslaw Trofimenko have had a huge impact on inorganic chemistry, with applications in fields such as catalysis, bioinorganic and materials chemistry [1,2]. The versatility of the scorpionate framework, which is elegant in its simplicity, has allowed hundreds of variants to be prepared. Important milestones in the history of scorpionate ligands include bulky "second generation" tris(pyrazolyl)borates, chiral scorpionates, highly electron-deficient tris(pyrazolyl)borates and scorpionates that are not based on pyrazolyl donors.

Bulky scorpionate ligands are able to stabilize four-coordinate pseudo-tetrahedral nickel complexes. Nickel complexes supported by ligands such as tris(pyrazolyl)borates [3,4], tris(phosphino)borates [5], tris(thioether)borates [6] and tris(mercaptoimidazolyl)borates [7], have been reported. Among these complexes are four-coordinate nickel nitrosyls, which allow the scorpionate ligand donor strength to be probed by the measurement of $\nu$(NO) [3–5,8]. In addition to allowing for comparisons of scorpionate donor strengths, tetrahedral nickel nitrosyl complexes also allow comparison with other ligands, including phosphines and cyclopentadienyls [9–11].

Some of us have been investigating metal complexes supported by bulky tris(carbene)borates [12–17]. We have shown the superior donor abilities of the tris(carbene)borate ligands in manganese carbonyl complexes [18]. We have also reported the synthesis of a square-planar nickel(II) bis(carbene)borate complex supported by bis(carbene)borate ligand [19]. In this report, we show that a bulky tris(carbene)borate ligand stabilizes four-coordinate nickel bromide [HB($^t$BuIm)$_3$NiBr] and nickel nitrosyl [HB($^t$BuIm)$_3$Ni(NO)] complexes. These complexes have been structurally and spectroscopically characterized, which has allowed us to quantify the bonding properties of this ligand. In particular, [HB($^t$BuIm)$_3$NiBr] has been investigated by high-frequency and -field electron paramagnetic resonance (HFEPR) and electronic spectroscopy, while [HB($^t$BuIm)$_3$Ni(NO)] has been investigated by IR spectroscopy. Furthermore, a series of tris(carbene)borate nickel nitrosyl complexes have been spectroscopically investigated to determine the effect of the tris(carbene)borate substituents on the donor strength of the ligand.

* Corresponding author. Tel.: +1 575 646 3346.
*E-mail address:* jesmith@nmsu.edu (J.M. Smith).

0020-1693/$ - see front matter © 2009 Elsevier B.V. All rights reserved.
doi:10.1016/j.ica.2009.05.015

## 2. Experimental

### 2.1. General synthetic procedures

All manipulations were performed under a nitrogen atmosphere by standard Schlenk techniques or in an M. Braun Labmaster glove box maintained at or below 1 ppm $O_2$ and $H_2O$. Glassware was dried at 150 °C overnight. Tetrahydrofuran, toluene and pentane were purified by the Glass Contour solvent purification system. Deuterated benzene was first dried over $CaH_2$, then over Na/benzophenone, and then vacuum transferred into a storage container. Before use, an aliquot of each solvent was tested with a drop of sodium benzophenone ketyl in THF solution. Celite was dried overnight at 200 °C. HB($^t$BuImH)$_3$(Br)$_2$ [12], PhB($^t$BuImH)$_3$(OTf)$_2$ [13], PhB(MesImH)$_3$(OTf)$_2$ [13], PhB(MeImH)$_3$(OTf)$_2$ [18] $NiBr_2(PPh_3)_2$ [20] and $NiBr(NO)(PPh_3)_2$ [9] were prepared according to literature procedures. Solid lithium diisopropylamide (LDA) was prepared by addition of $^n$BuLi to a solution of diisopropylamine in *n*-pentane at −78 °C, filtered, and stored at −35 °C. All other chemicals were obtained commercially and used as received.

### 2.2. Synthesis of HB($^t$BuIm)$_3$NiBr (**3**)

Lithium diisopropylamide (169 mg, 1.58 mmol) was added to a slurry of HB($^t$BuImH)$_3$(Br)$_2$ (275 mg, 0.51 mmol) in THF (15 mL). After stirring for 1 h, a slurry of $NiBr_2(PPh_3)_2$ (378 mg, 0.51 mmol) in THF (5 mL) was added to the reaction. The mixture was stirred at room temperature for 1 d, and dried under vacuum. The residue was extracted with toluene, filtered through Celite, dried under vacuum, washed with copious amounts of pentane and dried under vacuum to yield a light orange solid (140 mg, 53%). Crystals suitable for X-ray diffraction were obtained from toluene at −35 °C. $^1$H NMR (400 MHz, $C_6D_6$): $\delta$ = 103.6 (3H, HB($^t$Bu*Im*)$_3$), 11.8 (3H, HB($^t$Bu*Im*)$_3$), 5.3 (27 H, HB($^t$*Bu*Im)$_3$) and −8.4 (1H, *H*B($^t$BuIm)$_3$) ppm. IR (liquid cell, toluene, cm$^{-1}$): 2412 (w, B–H). APCI$^+$−MS 519 ($^{77}$Br), 521 ($^{79}$Br) ($C_{21}H_{34}N_6BNiBr^+$). $\mu_{eff}$(Evans', $C_6D_6$, 288 K): 2.5(3) B.M. Elemental Anal. Calc. for $C_{21}H_{34}N_6BNiBr$: C, 47.71; H, 6.48; N, 15.90. Found: C, 47.62; H, 6.95; N, 15.57%.

### 2.3. Synthesis of HB($^t$BuIm)$_3$Ni(NO)(**4**) and alkyl/aryl substituted analogs

Lithium diisopropylamide (153 mg, 1.43 mmol) was added to a slurry of HB($^t$BuImH)$_3$(Br)$_2$ (250 mg, 0.46 mmol) in THF (15 mL). After stirring for 1 h, a slurry of $NiBr(NO)(PPh_3)_2$ (318 mg, 0.46 mmol) in THF (5 mL) was added to the reaction. The mixture was stirred at room temperature for 1 d, and dried under vacuum. The residue was extracted with toluene, filtered through Celite, dried under vacuum, washed with copious amounts of pentane, and dried under vacuum to yield a deep purple solid (180 mg, 84%). $^1$H NMR (400 MHz, $C_6D_6$): $\delta$ = 6.97 (s, 3H, HB($^t$Bu*Im*)$_3$), 6.65 (s, 3H, HB($^t$Bu*Im*)$_3$), 4.5 (br. quartet, $J_{B-H}$ = 81 Hz, 1H, *H*B($^t$BuIm)$_3$) and 1.68 (s, 27H, HB($^t$*Bu*Im)$_3$) ppm. IR (liquid cell, toluene, cm$^{-1}$): 2411 (w, B–H), 1703 (s, N–O). APCI$^+$−MS 470 ($C_{21}H_{34}N_7BNiO^+$). Elemental Anal. Calc. for $C_{21}H_{34}N_7BNiO$: C, 53.66; H, 7.29; N, 20.86. Found: C, 53.31; H, 7.40; N, 20.70%. Crystals suitable for X-ray diffraction were obtained from a saturated toluene solution at −35 °C.

The other nitrosyl complexes were prepared by the same procedure.

*PhB($^t$BuIm)$_3$Ni(NO):* deep purple solid, 78% yield. $^1$H NMR (400 MHz, $C_6D_6$): $\delta$ = 8.05 & 8.04 (d, $J_{C-H}$ = 7.9 Hz, 2H, *Ph*B($^t$BuIm)$_3$, *o*-H), 7.38 (t, $J_{C-H}$ = 6.8 and 7.5 Hz, 3H, *Ph*B($^t$BuIm)$_3$, *p/m*-H), 6.97 (s, 3H, PhB($^t$Bu*Im*)$_3$), 6.68 (s, 3H, PhB($^t$Bu*Im*)$_3$) and 1.69 (s, 27H, PhB($^t$*Bu*Im)$_3$) ppm. IR (liquid cell, toluene, cm$^{-1}$): 1701 (s, N–O). APCI$^+$-MS 546 ($C_{27}H_{38}N_7BNiO^+$).

*PhB(MesIm)$_3$Ni(NO):* dark orange solid, 57% yield. $^1$H NMR (400 MHz, $C_6D_6$): $\delta$ = 8.10 and 8.08 (d, $J_{C-H}$ = 6.6 Hz, 2H, *Ph*B(MesIm)$_3$, *o*-H), 7.42 (t, $J_{C-H}$ = 6.6 and 7.4 Hz, 3H, *Ph*B(MesIm)$_3$, *p/m*-H), 7.11 (s, 3H, PhB(Mes*Im*)$_3$), 6.67 (s, 6H, PhB(*Mes*Im)$_3$, *m*-H) 6.40 (s, 3H, PhB(Mes*Im*)$_3$), 2.12 (s, 18H, PhB(*Mes*Im)$_3$, *o*-$CH_3$) and 1.97 (s, 9H, PhB(*Mes*Im)$_3$, *p*-$CH_3$) ppm. IR (liquid cell, toluene, cm$^{-1}$): 1724 (s, N–O). APCI$^+$−MS 733 ($C_{42}H_{45}N_7BNiO^+$).

*PhB(MeIm)$_3$Ni(NO):* light orange solid, 65% yield. $^1$H NMR (400 MHz, $C_6D_6$) $\delta$ = 7.99 and 7.97 (d, 2H, *Ph*B(MeIm)$_3$, *o*-H), 7.39 (t, 3H, *Ph*B(MeIm)$_3$, *p/m*-H), 6.91 (s, 3H, PhB(Me*Im*)$_3$), 6.10 (s, 3H, PhB(Me*Im*)$_3$) and 3.52 (s, 9H, PhB(*Me*Im)$_3$) ppm. IR (liquid cell, toluene, cm$^{-1}$): 1697 (s, N–O). APCI$^+$−MS 420 ($C_{18}H_{20}N_7BNiO^+$).

### 2.4. Crystal data collection and refinement

Crystals of **3** and **4** were coated in Paratone-N oil. For **3** a crystal of dimensions 0.13 × 0.13 × 0.02 mm was mounted on a standard Bruker X8 Apex2 CCD-based X-ray diffractometer equipped with an Oxford Cryostream 700 low temperature device and normal focus Mo-target X-ray tube ($\lambda$ = 0.71073 Å) operated at 1500 W power (50 kV, 30 mA). The X-ray intensities were measured at 223(2) K; the detector was placed at a distance 5.00 cm from the crystal. A full sphere of data consisting of 2511 frames was collected with a scan width of 0.5° in omega and phi with an exposure time of 22 s/frame. The frames were integrated with the Bruker SAINT software package with a narrow frame algorithm. Analysis of the data showed negligible decay during data collection; the data were processed with SADABS and corrected for absorption.

A red-violet rhombohedral plate of **4** measuring 0.28 × 0.230 × 0.253 mm was mounted on a standard Bruker X8 Apex2 CCD-based X-ray diffractometer equipped with an Oxford Cryostream 700 low temperature device and normal focus Mo-target X-ray tube ($\lambda$ = 0.71073 Å) operated at 1500 W power (50 kV, 30 mA). For data collection, the X-ray intensities were measured at 228(2) K; the detector was placed at a distance 5.50 cm from the crystal. A full sphere of data consisting of 2763 frames was collected with a scan width of 0.5° in omega and phi with an exposure time of 20 s/frame. The data integrated with the Bruker SAINT software package with a narrow frame algorithm. Analysis of the data showed negligible decay during data collection; the data were processed with SADABS and corrected for absorption.

Crystal and structural refinement data for **3** and **4** are shown in Table 1.

### 2.5. HFEPR spectroscopy

HFEPR spectra were recorded using the Millimeter and Sub-millimeter Wave Facility at NHMFL, and the EMR Facility. The former experimental setup employs backward wave oscillators generating tunable frequencies in the 70 GHz–1.2 THz range (of which the 120–700 GHz range was used in this study) and the resistive "Keck" magnet enabling 0–25 T field sweeps [21], while the latter utilizes a variety of solid-state sources and a superconducting 15/17 T magnet [22]. Detection was provided with an InSb hot-electron bolometer (QMC Ltd., Cardiff, UK). Modulation for detection purposes was provided alternatively by chopping the sub-THz wave beam ("optical modulation"), which produced an absorptive shape of the spectra, or by modulating the magnetic field, which delivered the more standard first derivative shape. A Stanford Research Systems SR830 lock-in amplifier converted the modulated signal to DC voltage.

### 2.6. Electronic absorption spectroscopy

UV–Vis spectra (230–800 nm) were recorded in Suprasil cuvettes at ambient temperature in THF and in $CH_2Cl_2$ solutions on

**Table 1**
Crystal data and structure refinements for complexes **3** and **4**.

| | **3** | **4** |
|---|---|---|
| Formula | $C_{27}H_{37}BBrN_6Ni$ | $C_{21}H_{136}BN_7NiO{\cdot}0.7$ |
| Formula weight | 594.73 | 571.50 |
| $T$ (K) | 223(2) | 293(2) |
| Wavelength (Å) | 0.71073 | 0.71073 |
| Crystal system | Orthorhombic | Orthorhombic |
| Space group | $P21\ c\ n$ (No. 33) | $P21\ c\ n$ (No. 33) |
| $a$ (Å) | 10.0730 (3) | 19.0361(19) |
| $b$ (Å) | 16.0245 (5) | 15.8574(14) |
| $c$ (Å) | 19.0091 (6) | 10.1809(10) |
| $\alpha$ (°) | 90 | 90 |
| $\beta$ (°) | 90 | 90 |
| $\gamma$ (°) | 90 | 90 |
| $V$ (Å$^3$) | 3068.35(16) | 3073.2(5) |
| $Z$ | 4 | 4 |
| $D_{calc}$ (g cm$^{-3}$) | 1.224 | 1.152 |
| $\mu$(Mo K$\alpha$) (mm$^{-1}$) | 1.955 | 0.660 |
| $F$(0 0 0) | 1178 | 1126 |
| Crystal size (mm) | 0.13 × 0.13 × 0.02 | 0.28 × 0.25 × 0.23 |
| Theta range for data collection (°) | 1.66–20.00 | 1.67–21.50 |
| Limiting indices | $-9 \leqslant h \leqslant 9$, $-15 \leqslant k \leqslant 15$, $-18 \leqslant l \leqslant 18$ | $-10 \leqslant h \leqslant 10$, $-16 \leqslant k \leqslant 16$, $-19 \leqslant l \leqslant 19$ |
| Reflections collected/unique [$R_{(int)}$] | 23 813/2825 [0.0652] | 22 412/3533 [0.0261] |
| Refinement method | Full-matrix least-squares on $F^2$ | Full-matrix least-squares on $F^2$ |
| Data/parameters | 2825/278 | 3533/345 |
| Goodness-of-fit on $F^2$ | 1.197 | 1.264 |
| Final $R$ indices [$I > 2\sigma(I)$] | $R_1 = 0.0568$, $wR_2 = 0.1623$ | $R_1 = 0.0366$, $wR_2 = 0.1067$ |
| $R$ indices (all data) | $R_1 = 0.0669$, $wR_2 = 0.1780$ | $R_1 = 0.0437$, $wR_2 = 0.1198$ |
| Extinction coefficient | 0.0130(11) | 0.0122(11) |
| Largest difference in peak/hole (e/Å$^3$) | 0.415/−0.665 | 0.867/−0.606 |

either CARY 100 Bio UV–Vis (NMSU) or Jasco 570 (Roosevelt U.) spectrophotometers. The latter instrument was also used to record NIR spectra (800–2500 nm) of **3** in THF-$d_8$ and $CD_2Cl_2$ solution. These solvent isotopologs were chosen to minimize interference from $\nu$(C–H) overtones in the NIR region.

### 2.7. Other experimental procedures

NMR data were recorded on a Varian Unity 400 spectrometer (400 MHz) at 22 °C. All peaks in the $^1$H NMR spectra are referenced to residual $C_6D_5H$ at $\delta$ 7.16 ppm. Solution magnetic susceptibilities were determined by the Evans method [23]. Mid-IR spectra were recorded on a Perkin–Elmer Spectrum One FTIR spectrophotometer in toluene solution. Atmospheric pressure positive ionization mass spectral data were collected using a Waters-Micromass ZQ2000 Mass Spectrometer. Elemental analysis data was collected by Robertson Microlit Laboratories, Madison, NJ.

### 2.8. Spectroscopic analysis procedures

Details of the tunable-frequency EPR methodology employed to analyze HFEPR spectra recorded for **3** are given elsewhere [24]. This procedure includes analysis of the field versus frequency dependence of turning points in powder-patterned multi-frequency spectra, which were fitted by a non-linear least squares procedure based on exact solutions for energies of the triplet state [25]. Simulation of individual HFEPR spectra including nuclear interactions (hyperfine and quadrupole coupling) employed the program DDPOWHE (available from J. Telser) which calculates transition energies and intensities by matrix diagonalization [26].

### 2.9. Ligand-field analysis procedures

Analysis of the electronic structure of Ni(II) in the studied complexes was performed with use of the angular overlap model (AOM) [27]. Two computer programs were employed, LIGFIELD, written by J. Bendix (Ørsted Institute, Copenhagen, Denmark) [28] and a locally-written program, DDN, available from J. Telser. Both programs use the complete $d^8$ (equivalent to $d^2$) weak-field basis set including inter-electronic repulsion (Racah parameters: $B$, $C$), spin–orbit coupling (SOC constant: $\zeta$) [28] and AOM ligand-field bonding parameters ($\varepsilon_\sigma$, $\varepsilon_\pi$), and gave identical results when directly compared. DDN allows use of a non-linear least-squares fitting subroutine (DSTEPIT, from QCPE, Bloomington, IN) to match observed electronic transition energies to those calculated by user-defined variable parameters such as $B$, $\varepsilon_\sigma$, etc. The general AOM procedure involved an initial fit of spin-allowed optical transitions with variation of Racah $B$ and AOM σ-bonding parameters, and with $\zeta \equiv 0$. The bromo ligand was considered to have cylindrical π-donation as well; π-bonding involving the carbene donors was explored as described in Section 3.6. To make the fitting tractable, the bonding parameters for the three carbene (imidazolylidene) donors were held identical (i.e., imposed $C_3$ bonding symmetry). From this initial fit, $\zeta$ was systematically varied until a reasonable match obtained for $|D|$ in relation to experimental values. The resulting electronic transitions were then checked to ensure that they were still in agreement with experiment.

## 3. Results and discussion

### 3.1. General synthetic rationale

Shown in Scheme 1 is the synthesis of a bulky tris(carbene)borate ligand and its nickel(II) complexes. The synthesis of the ligand precursor salt, $HB(^tBuImH)_3(Br)_2$ (**1**) has been previously described [12]. Initially, we attempted to prepare nickel(II) complexes using $HB(^tBuIm)_3MgBr$ [12] as a ligand transfer agent. However, reaction between the magnesium complex and various nickel sources (e.g., $NiBr_2$, $NiCl_2$(DME) and $NiBr_2(PPh_3)_2$) led to a mixture of uncharacterized products and unreacted starting material.

Given the success in preparing a nickel bis(carbene)borate complex from a lithium bis(carbene)borate ligand transfer reagent [19] we targeted an analogous lithium tris(carbene)borate for ligand transfer to nickel(II).

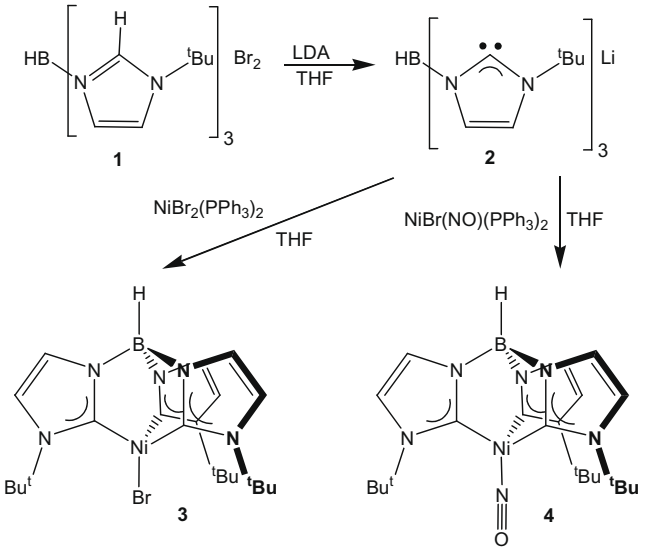


**Scheme 1.**

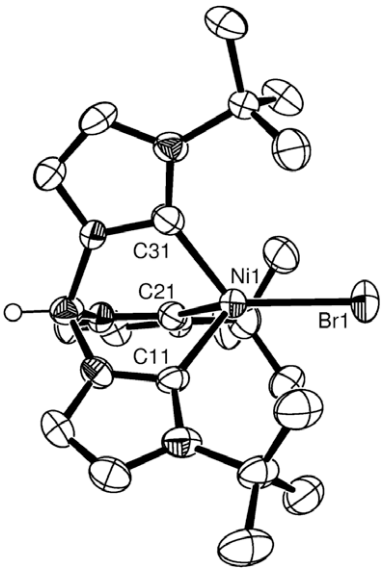


**Fig. 1.** ORTEP diagram of HB($^t$BuIm)$_3$NiBr (**3**) with hydrogen atoms removed for clarity. Thermal ellipsoids shown are at 50% probability.

Deprotonation of **1** with LDA to yield the lithium complex "HB($^t$BuIm)$_3$Li" (**2**) occurred within an hour at room temperature as determined by $^1$H NMR spectroscopy. The key marker is the disappearance of the acidic hydrogen peak at $\delta$ 9.73 ppm in the $^1$H NMR spectrum. A similar spectral change was observed in the synthesis of a lithium bis(carbene)borate complex [19]. The lithium tris(carbene)borate complex **2** has similar solubility properties as the lithium bis(carbene)borate complex (e.g., soluble in THF and $Et_2O$) [19].

### 3.2. Synthesis and structural characterization of HB($^t$BuIm)$_3$NiBr (**3**)

Reaction of *in situ* prepared **2** with $NiBr_2(PPh_3)_2$ [20] led to the formation of an orange solid, which was isolated in 53% yield after workup. Other nickel(II) sources (e.g., $NiBr_2$, $NiCl_2$, and $NiCl_2$(DME)) led to the formation of multiple products.

The orange solid was characterized as HB($^t$BuIm)$_3$NiBr (**3**) by X-ray crystallography. The X-ray crystal structure of **3** confirms a monomeric four-coordinate nickel species (Fig. 1). The tris(carbene)borate ligand is coordinated to the nickel center in a tridentate fashion, with the bulky *tert*-butyl groups of the ligand helping to create a pseudo tetrahedral configuration by preventing the coordination of a second scorpionate ligand to the metal center. Selected metrical parameters for the crystal structure of **3** are shown in Table 2.

The crystal structure of **3** is isomorphous with that of the iron complex HB($^t$BuIm)$_3$FeBr [15]. The most significant differences between the two structures are the longer bond lengths between the metal and ligands (both metal–carbene ligand and metal–bromide bonds) of the iron complex, which can be attributed to the larger ionic radius of iron(II) as compared to nickel(II) (Table 2).

Complex **3** is isostructural with hydrotris(3-*tert*-butylpyrazolyl)borate nickel(II) chloride, Tp$^{tBu}$NiCl[29] (Fig. 2). Interestingly, the Ni–C/N bond lengths in **3** and Tp$^{tBu}$NiCl are the same, in contrast to the Ni–N bond lengths in [Tp$^*$]NiBr (Tp$^*$ = hydrotris(3,5-dimethylpyrazolyl) [30], which are shorter than the Ni–C bond lengths in **3**. It is likely that the structural similarities of **3** and Tp$^{tBu}$NiCl are due to greater intramolecular steric congestion created by the Tp$^{tBu}$ as compared with the Tp$^*$ ligand.

### 3.3. Fluid solution NMR studies of **3**

The magnetic moment of the nickel complex was determined by the Evans method to be 2.5(3) B.M., which is consistent with $S = 1$, as expected for a pseudo-tetrahedral complex of Ni(II). The ambient temperature $^1$H NMR spectrum of **3** is also consistent with this description. Such a system readily gives $^1$H NMR spectra with extensive paramagnetic shifts, both positive and negative [31–33].

**Table 2**
Selected bond lengths (Å) and angles (°) from the X-ray crystal structures of **3** and related complexes.

| Distance/angle | HB($^t$BuIm)$_3$NiBr (**3**)[a] | HB($^t$BuIm)$_3$FeBr[b] | [Tp$^{tBu}$]NiCl[c] | [Tp$^*$]NiBr[d] |
|---|---|---|---|---|
| M–C/N | 2.028(7) | 2.135(3) | 2.033(3) | 1.957(6), 1.987(5) |
| | 2.031(9) | 2.123(3) | 2.006(4) | 1.968(4), 1.966(4) |
| | 2.002(7) | 2.127(3) | 2.023(4) | 1.968(4), 1.966(4) |
| M–X | 2.3953(13) | 2.4432(6) | 2.172(2) | 2.2928(13), 2.2887(13) |
| C/N–M–C/N | 92.9(3) | 91.1(1) | 91.4(2) | 92.88(17), 93.14(16) |
| | 91.2(3) | 90.6(1) | 93.7(2) | 92.88(17), 93.14(16) |
| | 91.8(3) | 93.1(1) | 93.2(2) | 91.3(2), 91.3(2) |
| C/N–M–X | 123.2(2) | 125.85(9) | 125.4(1) | 122.77(19), 120.81(17) |
| | 122.5(2) | 125.63(8) | 125.0(1) | 124.00(12), 124.80(13) |
| | 125.9(2) | 122.91(9) | 119.4(1) | 124.00(12), 124.80(13) |

[a] This work.
[b] Reported by Nieto et al. [12].
[c] Reported by Belderraín et al. [29].
[d] Reported by Desrochers et al. [30].

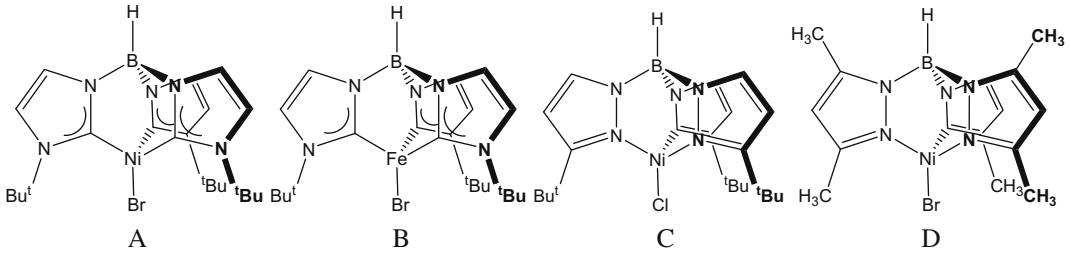


**Fig. 2.** Molecular structures of **3** (A); HB($^t$BuIm)$_3$FeBr (B) [15]; [Tp$^{t\mathrm{Bu}}$]NiCl (C) [29]; [Tp$^*$]NiBr (D) [30].

The $^1$H NMR spectrum has two resonances at $\delta = +103.6$ and +11.8 ppm that are assigned to the imidazol-2-ylidene groups, a very broad resonance at $\delta = +5.3$ ppm assigned to the *tert*-butyl groups and one resonance from the BH group at $\delta = -8.4$ ppm. All these resonances are assigned on the basis of integration. Qualitatively, the large positive shift of one of the imidazol-2-ylidene protons and the negative shift of the hydroborate proton indicate electron spin delocalization throughout the ligand. Future computational studies will address the NMR data quantitatively as extensive orbital contributions to the electron magnetic moment (as manifest in the zfs described below in Section 3.4) make this a complicated situation [31–33].

### 3.4. HFEPR spectroscopy of solid **3**

Complex **3** produced well-defined HFEPR spectra characteristic for a triplet state powder pattern in all the available frequency range (Fig. 3). Each spectrum consisted of a nominally forbidden $\Delta M_S = \pm 2$ transition, represented in the powder pattern by the so-called "half-field" or $B_{min}$ turning point, and two allowed $\Delta M_S = \pm 1$ transitions, each represented with up to three turning points representing the *x*, *y* and *z* orientations of the zfs tensor of each complex relative to the magnetic field. These turning points are superimposed on the broad absorption pattern centered on $g \sim 2.2$ at each frequency. There is an additional sharp peak at $g \sim 2.2$ in the experimental spectra, which is the so-called "double-quantum transition" that is very characteristic for Ni(II) complexes [34] and is not analyzed further. To analyze the rich set of resonances, we created a 2D field versus frequency map of the turning points (Fig. 4), and fitted the parameters of the usual spin Hamiltonian:

$$\mathscr{H} = \beta B \cdot \mathbf{g} \cdot S + D(S_z^2 - S(S+1)/3) + E(S_x^2 - S_y^2) \quad (1)$$

to the observed dependencies. The resulting values: $S = 1$, $|D| = 2.49(4)\,\mathrm{cm}^{-1}$, $|E| = 0.54(2)\,\mathrm{cm}^{-1}$, $g_x = 2.22(1)$, $g_y = g_z = 2.21(1)$ were used to calculate the curves in Fig. 4. A high rhombicity of the zfs tensor ($|E/D| \sim 0.2$) is noted at this point. To obtain the sign of *D*, we simulated single-frequency spectra rather than the complete 2D dataset, at different temperatures. An example of such a procedure is shown in Fig. 5. While it is difficult to get an unequivocal conclusion from the spectrum recorded at 30 K, the spectrum taken at 5 K shows more similarity with a simulation using a negative value of *D* than that produced with a positive *D*. Moreover, the trend of particular turning points changing intensity between 5 and 30 K agrees better with the simulations assuming a negative *D*. The zfs parameter *E* is by convention attributed the same sign as *D*, i.e., in this case negative.

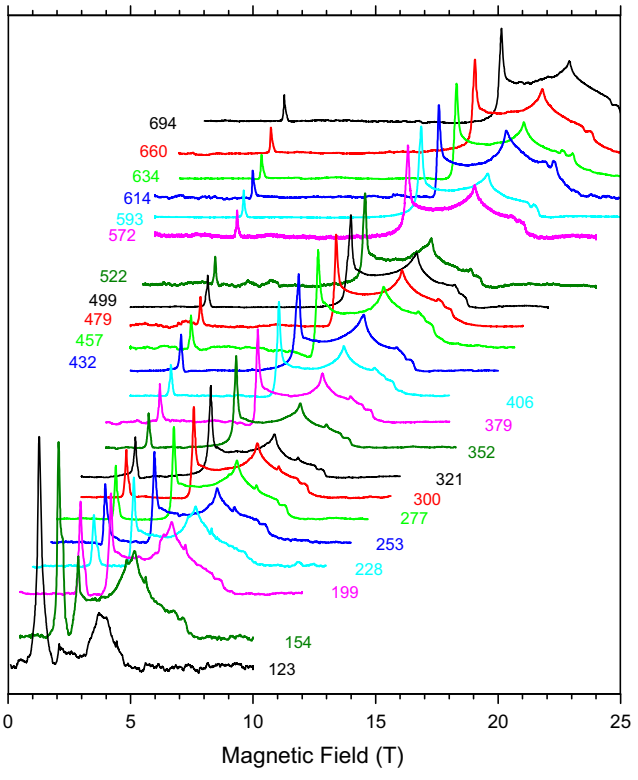


**Fig. 3.** A multi-frequency set of HFEPR spectra of microcrystalline **3** recorded at 4.2 K using optical modulation (i.e., in absorptive mode). The frequencies (in GHz) are given adjacent to each spectrum.

The derivative shape of the magnetically modulated spectra brought about an unexpected result, namely a field-independent structure superimposed on the $B_{min}$ peak (but not $\Delta M_S = \pm 1$ transitions) in a limited range of frequencies and temperature (Fig. 6). The optimal resolution of that structure was obtained between 300 and 440 GHz, and around 30 K. The lack of field dependence of this structure (other than the broadening "strain" effects) can point to its origin only from the hyperfine interaction between the electron and nuclear spin(s) of some proximate nucleus or nuclei. The lack of an identical structure on the $\Delta M_S = \pm 1$ transitions can be explained by the fact that the latter are strongly anisotropic while the "half-field resonance" (which is an off-axis turning point of the $\Delta M_S = \pm 2$ transition) is almost isotropic. Thus, field-induced strain phenomena may have a much stronger influence on the former than the latter. The observation of a nicely resolved hyperfine pattern is, to our best knowledge, the first in HFEPR spectra of a *magnetically undiluted* solid-state complex, and in particular, one with integer spin (non-Kramers ion). Hyperfine structure has been detected in HFEPR studies of *magnetically diluted single crystals* of Cs/Ga alums doped with either V(III) ($3d^2$, $S = 1$) [35], or Mn(III) ($3d^4$, $S = 2$) [36]. These systems exhibited well resolved couplings from $^{51}$V and $^{55}$Mn, respectively. In these cases, the combination of axial symmetry, magnetic dilution, and a single molecular orientation afforded narrow lines and resolved splitting. The only other example of hyperfine structure observation in a magnetically undiluted solid-state complex, both as a powder and single crystal,

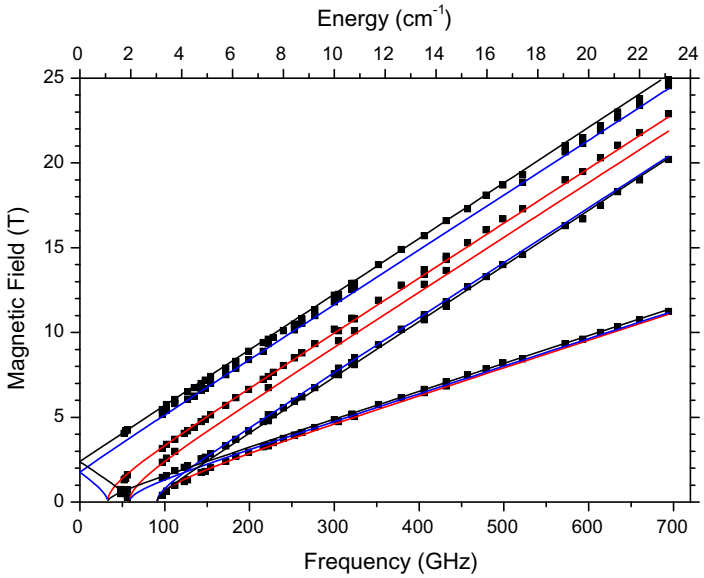


**Fig. 4.** 2D field versus frequency (or energy) map of turning points recognized in the HFEPR spectra of **3** shown in Fig. 3. Squares are experimental resonances while curves were generated using best-fitted spin Hamiltonian parameters: $S = 1$, $|D| = 2.49\ cm^{-1}$, $|E| = 0.54\ cm^{-1}$, $g_x = 2.22$, $g_{y,z} = 2.21$. Red curves correspond to turning points with $B_0||x$, blue curves – with $B_0||y$, and black curves – with $B_0||z$. (For interpretation of the references to colour in this figure legend, the reader is referred to the web version of this article.)

known to us is the very recent experiment on a complex of rhenium(IV) ($5d^3$), $(Bu_4N)_2[ReCl_4(ox)]$, a Kramers system with $S = 3/2$ [37]. More typically, powder pattern HFEPR spectra exhibit broad unresolved lines even with magnetic dilution [24].

The magnitude of the hyperfine constant, on the order of 1.5 GHz, suggests that the coupling is due to a heavy nucleus. There is only one such nucleus directly neighboring the paramagnetic center in **3**, and that is bromine ($^{79,81}Br$, $I = 3/2$, respectively 50.69% and 49.31% abundant, with $g_N$ for the former isotope 93% of that for the latter). Large hyperfine coupling from a nominally closed-shell "innocent" ligand is surprising, yet we see no other explanation.[1] The interpretation of the observed hyperfine pattern is, however, nontrivial. The six-line pattern is not that expected for a single nucleus with $I = 3/2$, namely a 1:1:1:1 quartet, yet there is but a single bromine ligand in the complex. It is known that hyperfine powder patterns can be difficult to understand; a full interpretation of the structure observed in **3** may thus not be feasible without performing an experiment on a single crystal. However, we did make attempts to reproduce the observed pattern by simulations using the full spin Hamiltonian for an $S = 1$ system with a coupled $I > 1/2$ nucleus:

$$\mathscr{H} = \beta B \cdot \mathbf{g} \cdot S + D(S_z^2 - S(S+1)/3) + E(S_x^2 - S_y^2) + \beta_N g_N B \cdot I + S \cdot \mathbf{A} \cdot I + I \cdot \mathbf{P} \cdot I \quad (2)$$

where the last three terms involve the nucleus and are the isotropic Zeeman, and anisotropic hyperfine and quadrupole interactions, respectively. Simulations were performed separately for $^{79}Br$ and $^{81}Br$ and summed in the appropriate abundance ratio. The nuclear parameters we used to optimize the similarity of simulations to experiment: $A_{iso}(^{81}Br) = 1.50$ GHz ($A_{iso}(^{79}Br) = 1.39$ GHz), $P_{||}(^{81}Br) = (3/2)P_z = 33$ MHz ($P_{||}(^{79}Br) = 40$ MHz) were based on several earlier studies of analogous complexes. These included NQR studies on Ni(II) bromo complexes with $S = 0$ and 1 [39,40], which yielded quadrupole coupling parameters and single-crystal EPR studies of Ni(I) doped Cu(I) bromo complexes [41], which yielded hyperfine couplings.

The most successful simulation resulted from the superposition of three signals with isotropic hyperfine coupling and slightly different isotropic $g$ values (each offset by 0.05 T, $g_{eff} \sim 0.03$ from its neighbor(s)), so that the superposition of the three quartet patterns gives the observed six-line pattern. The result is shown in Fig. 7 for the feature at 432 GHz, where signal-to-noise and resolution are optimal. We realize that this is a phenomenological model; the position of $B_{min}$ depends on both the **g** matrix and the **D** tensor [42], (p. 165) and it is highly likely that $\mathbf{A}(^{79,81}Br)$ is also anisotropic. Apparently, a combination of these interactions, along with possible heterogeneity in the powder sample, contributes to give the observed pattern at $B_{min}$. If we assume that the isotropic hyperfine coupling derived from the simulations, $a_{iso}(^{81}Br) \approx 1.5(0.1)$ GHz, is correct, then this means that there is substantial spin delocalization onto the bromo ligand. The isotropic hyperfine coupling, $a_0(^{81}Br)$, corresponding to an unpaired electron in a $^{81}Br$ 4s orbital, equals 34.57 GHz [42]. Smith and Stoessiger, in their NQR study of $NiBr_2(PPh_3)_2$, assumed 15% s character in the Br bond to Ni [39], rather less than ideal $sp^3$ hybridization. If the unpaired spin were of this type, i.e., a model in which the Ni–Br portion of the complex were described not as Ni(II) and $Br^-$, but as Ni(I) and Br·, then $a_{iso}(^{81}Br) \approx 5.2$ GHz. The observed coupling is roughly a third of this value (~20% if $sp^3$ is used), indicating a substantial contribution of this delocalization description. Due to the inability to extract anisotropy in the hyperfine coupling from a powder spectrum, in contrast to a single-crystal study [41], we cannot unravel the anisotropic contribution to hyperfine coupling from spin delocalization into 4p orbitals. The bromine hyperfine coupling in $NiBr(PPh_3)_2 \cdot 0.5C_6H_6$ is much smaller in magnitude ($A_{max} \sim 93$ MHz) than in **3**, and is indeed very anisotropic, resulting from π-bonding [41]. This suggests not only that σ-donation from bromine in the Ni(I) complex is much less than in **3**, but also that the hyperfine coupling in **3** has anisotropy, which could lead to the observed six-line pattern. Future computational studies, hopefully combined with single-crystal HFEPR experiments, and other

[1] As A.C. Doyle attributed to S. Holmes, addressing J. Watson in "The Sign of Four": "How often have I said to you that when you have eliminated the impossible, whatever remains, however improbable, must be the truth [38]".

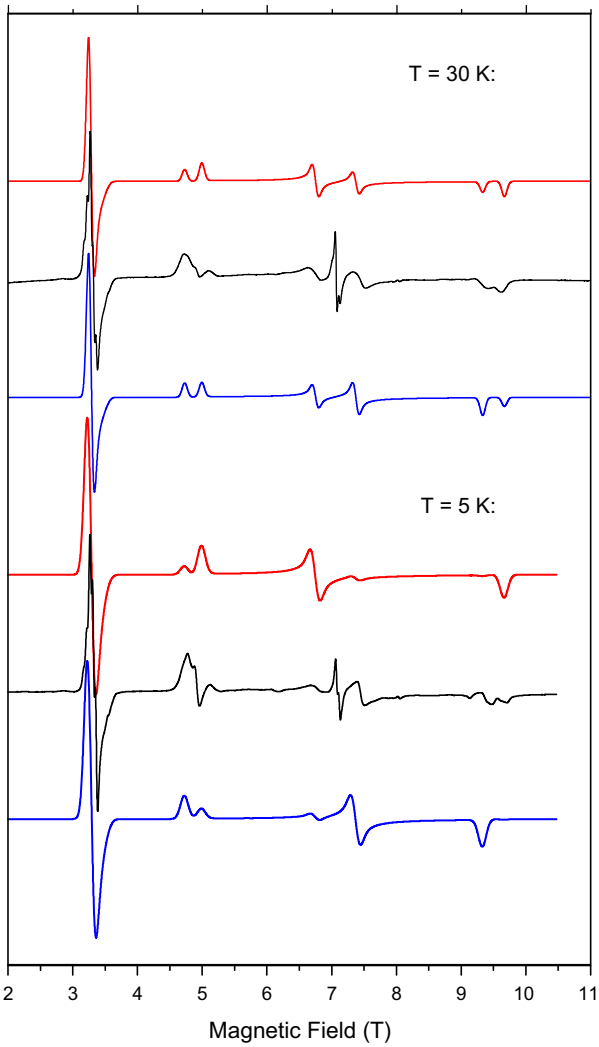


**Fig. 5.** HFEPR spectra recorded using magnetic modulation (i.e., in derivative mode) at 222.4 GHz at 5 K (lower solid trace) and 30 K (upper solid trace) accompanied by powder-pattern simulations using the following spin Hamiltonian parameters: $S = 1$, $|D| = 2.52$, $|E| = 0.63\ cm^{-1}$, $g_{iso} = 2.22$. Dotted traces were calculated using positive values of the zfs parameters, while dashed traces – using negative values. The sharp peak at $g \sim 2.2$ (~7.2 T) in the experimental spectra is the so-called "double quantum transition" (see text), which is not simulated.

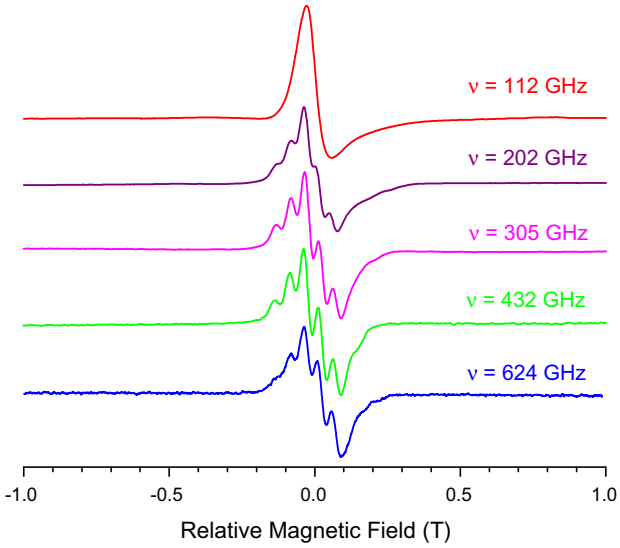


**Fig. 6.** The hyperfine structure superimposed on the $B_{min}$ turning point in the EPR spectra of **3** recorded using magnetic modulation at 30 K and various frequencies, as indicated. Zero on the magnetic field scale corresponds to 1.004 T at 112 GHz, 3.315 T at 202 GHz, 4.730 T at 305 GHz, 6.870 T at 432 GHz, and 10.012 T at 624 GHz.

spectroscopic techniques, such as MCD, along with the preparation and characterization of analogs to **3** will eventually address quantitatively the interesting question of spin delocalization.

### 3.5. Electronic absorption spectroscopy of *3*

The UV–Vis–NIR spectra of paramagnetic four-coordinate Ni(II) complexes have been previously analyzed by some of us [30,43], in particular [Tp*]NiBr [30]. It was thus of interest to compare these tris(pyrazolyl) complexes to the tris(carbene)borate complex [HB($^t$BuIm)$_3$NiBr], **3**. The UV spectrum of **3** exhibits a very strong, broad band centered at 275 nm ($\varepsilon = 4500\ M^{-1}\ cm^{-1}$), which is assigned to $\pi$–$\pi^*$ transitions involving the imidazol-2-ylidene groups, but may have LMCT character. There is also a band at 360 nm ($\varepsilon = 500\ M^{-1}\ cm^{-1}$), which does not have a corresponding band in Tp* complexes. Separate experimental and computational studies are in progress on the UV spectra of pyrazolyl and imidazolyl hydroborate anions with diamagnetic cations (e.g., Mg(II)). We focus here on the Vis–NIR region that directly involves the Ni ion.

Vis–NIR spectra recorded in both $CD_2Cl_2$ and THF-$d_8$ were essentially identical and are shown in Fig. 8; the UV–Vis spectrum is shown in Fig. S1. There are two bands in the Vis region: at 472 nm ($\varepsilon = 210\ M^{-1}\ cm^{-1}$) and at 738 nm ($\varepsilon = 290\ M^{-1}\ cm^{-1}$), which has a shoulder at 690 nm. There is one, broad band in the NIR region at 1360 nm ($\varepsilon = 170\ M^{-1}\ cm^{-1}$) which may have two components. These data are summarized in Table 3, which also presents data for [Tp*]NiBr, the complex most relevant to **3**. Qualitatively, the two complexes exhibit similar Vis–NIR spectra, except the bands for the imidazolylidene complex are all blue-shifted relative to the corresponding bands for the pyrazolyl complex. This is likely the consequence of the carbenes being stronger $\sigma$-donors than the imines. The band assignments made for [Tp*]NiBr, however, can be directly applied to **3**, as indicated in Table 3. The only ambiguity is that the transition $^3A_2(^3T_1, F) \rightarrow {}^3A_2(^3A_2, F)$ likely overlaps with MLCT and/or ligand-based transitions. This will be addressed in the studies of Mg(II) and other complexes as mentioned above.

### 3.6. Ligand-field theory (LFT) analysis of *3*

The complex [Tp*]NiBr was previously analyzed using the LFT AOM [30], based on the combination of structural and spectroscopic (Vis–NIR and HFEPR) data. The correspondence of the electronic absorption spectra of **3** with [Tp*]NiBr, suggested that the same procedure could be applied to this complex. The same molecular coordinate system was used, namely that the approximate $C_3$ axis defines the principal, $z$, direction. The Br–Ni–C bond angles define the angles $\theta$ used in the AOM. These three angles are not identical, but have a narrow range: 122.5°–125.9°, as seen in Table 2. The molecular $x$ direction was defined as lying along the Ni–C11 vector, which yields the $\varphi$ angles 121.44° and 240.65° for C21 and C31, respectively.

The solid state structure as applied to the AOM is thus close to threefold symmetry. Use of this model and $\sigma$-bonding parameters derived initially from those used for [Tp*]NiBr, but without any $\pi$-bonding, led to a successful fit to the electronic transitions. This fit yielded a value for the Racah parameter, $B = 557\ cm^{-1}$, 52% of the free-ion value [27], which is reasonable for such a covalent

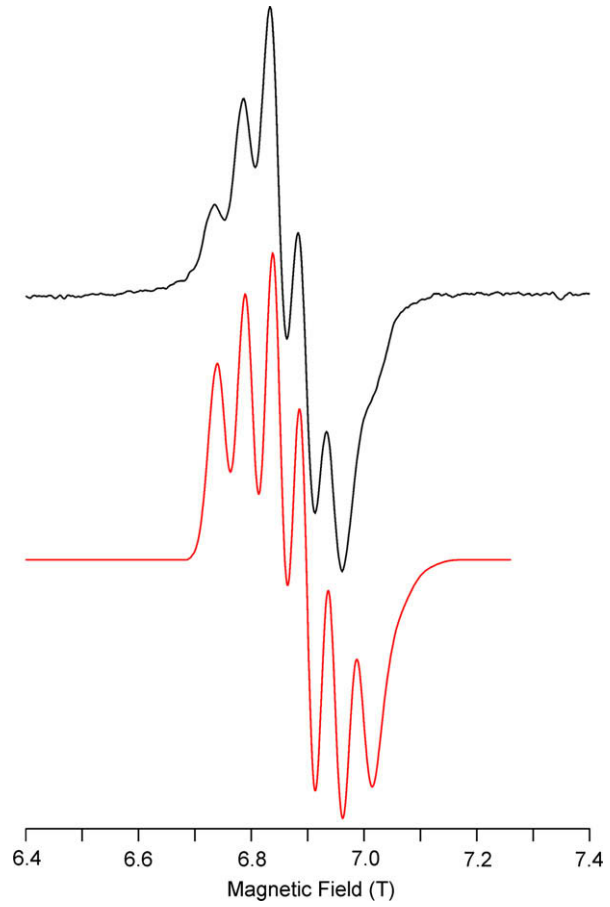


**Fig. 7.** Experimental HFEPR spectrum of **3** recorded using magnetic modulation at 30 K and at 432 GHz (upper trace) along with a simulation (lower trace), generated as the sum of three individual spectra with slightly varying $g_{iso}$ values: 2.230, 2.215, 2.200. Each simulation otherwise uses the following identical parameter set: $S = 1$, $D = +2.49\ cm^{-1}$, $E = +0.54\ cm^{-1}$; isotropic Gaussian linewidth (hwhh), 1.2 GHz; $A_{iso}(^{81}Br) = 1.50$ GHz ($A_{iso}(^{79}Br) = 1.39$ GHz), $P_{||}(^{81}Br) = (3/2)P_z = 33$ MHz ($P_{||}(^{79}Br) = 40$ MHz). Simulations were calculated for each Br isotope and then summed in the abundance ratio.

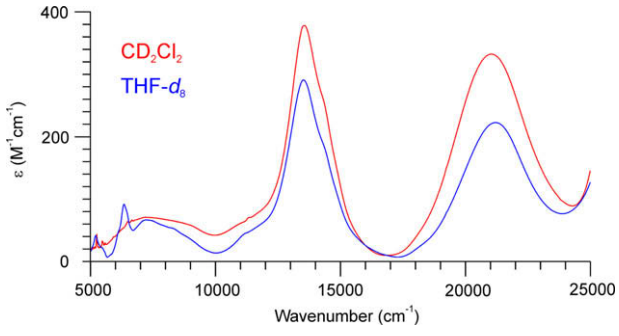


**Fig. 8.** Vis–NIR absorption spectrum of **3** in $CD_2Cl_2$ (solid trace) and THF-$d_8$ (dashed trace). The sharp bands at 6250 $cm^{-1}$ and 5200 $cm^{-1}$ are vibrational in origin from THF-$d_8$.

complex. The fit parameters are given in Table S1. As suggested by the Vis–NIR spectra, the imidazol-2-ylidene carbenes are significantly stronger σ-donors than are the pyrazolyl imines: $\varepsilon_\sigma = 6600\ cm^{-1}$ versus $5160\ cm^{-1}$. For comparison, Larrabee et al. reported $\varepsilon_\sigma = 4640\ cm^{-1}$ for pyrazolyl N-donors to four-coordinate high-spin Co(II) in $Tp^{R,R'}CoL$ (L = halogen, pseudohalogen; R, R′ = various alkyl/aryl pyrazole substituents) [44].

The possible contribution of π-bonding was also explored using the AOM. In the study on [Tp*]NiX (X = Cl, Br, I), π-donation involving the pyrazolyl ligands was included, which was based on earlier work by Fujihara et al. on $[Tp_2Cr]^+$ and $[Tp_2Co]^+$ [45]. However, the results for [Tp*]NiX were ambiguous in that inclusion of π-donation by the pyrazolyl ligands gave good fits to the electronic absorption spectra, but so did omission of this effect (π-acceptor behavior was not reasonable) [30], as we have reconfirmed here. Likewise, Larrabee et al. did not include any pyrazole π-bonding effects and were able to fully model the experimental absorption and MCD transitions of several $Tp^{R,R'}CoL$ complexes [44]. Disregarding possible twist angles, two orientations of π-bonding are possible, π-$c(x)$ and π-$s(y)$ [46]. In the coordinate system used here, π-$c(x)$ corresponds to π-bonding involving the central metal ion $d_{z^2}$, $d_{xz}$, $d_{yz}$ orbitals and π-$s(y)$ to $d_{xy}$, $d_{x^2-y^2}$. Fujihara et al., in their study of six-coordinate Cr(III) and Co(III) complexes, set π-$c(x) \equiv 0$ [45], and that was assumed in the [Tp*]NiX study as well [30]. For **3**, however, we did not wish to presume which orientation is optimal for π-bonding in these trigonal systems with a novel ligand. Nevertheless, inclusion of π-$c(x)$ bonding had a only minimal effect on the fit (see Table 3) and the resulting parameters suggested only slight π-acceptor properties (π-$c(x) \approx -120\ cm^{-1}$; see Table S1), which may be merely the consequence of an additional fit parameter. However, inclusion instead of π-$s(y)$ bonding for **3** had a significant effect and the resulting magnitude was relatively large (π-$s(y) \approx -1000\ cm^{-1}$; see Table S1); well outside the range of mere "tweaking" of a fit. Indeed, this magnitude of π-donation is comparable to that determined for other paramagnetic four-coordinate complexes of Ni(II), which have (cylindrical) $\varepsilon_\pi$ ranging from $-500$ to $-1500\ cm^{-1}$ [30,47,48]. The crude nature of the AOM as we and others have applied it makes a definitive conclusion impossible; however, it appears that in the classical scorpionate systems, namely four-coordinate mono(tris(pyrazolyl)borate) or six-coordinate bis(tris(pyrazolyl)borate) complexes, there are π-donor or non π-interacting scorpionate ligands, but in the four-coordinate mono(tris(carbene)borate) complex there may well be π-acceptor behavior, as found with phosphine complexes [47,48].

Although the π-bonding properties of N-heterocyclic carbene ligands were initially suggested to be negligible, π-acceptor behavior in electron-rich complexes has been proposed on the basis of electronic structure calculations [49,50]. Experimental support for this suggestion has come from investigations of iron(II) [51] and rhodium(I) [52–54] carbonyl complexes, wherein their $\nu$(CO) vibrational frequency was used as a reporter of π-acceptor ability. Our results, which are based on a totally unrelated technique, are nevertheless consistent with these proposals of π-acceptor behavior and furthermore provide an estimate of their π-acceptor ability. Investigations of other mono(tris(carbene)borate) and bis(tris(carbene)borate) complexes are in progress to test this proposal further.

The final concern is to include spin–orbit coupling and calculate zfs for comparison with experiment. In the case of the [Tp*]NiX series, this comparison was successful only for X = Cl, but was problematic for X = Br and I. In order to achieve the experimental zfs for [Tp*]NiBr ($D \approx 11\ cm^{-1}$), it was necessary to include an unrealistically large value for $\zeta$ (nearly the free-ion value; see Table S1) [30]. Furthermore, the calculated sign of $D$ was opposite to that obtained experimentally. A similarly problematic situation is found here for the bromo complex, **3**. The smaller zfs found here for **3** ($D \approx 2.5\ cm^{-1}$) means that a reasonable value for $\zeta$ is required, $\sim 285\ cm^{-1}$, which is only ~40% of the free-ion value [28]; a ratio similar to that found for *B*. However, this calculation clearly yields a positive sign for $D$, not the negative sign obtained from

**Table 3**
Electronic absorption transition energies ($cm^{-1}$) and molar absorptivities ($M^{-1}\,cm^{-1}$) (in parentheses) for **3** and related complexes.

| Assignment[a] | CT | CT | $^3A_2$ ($^3A_2$, F) | $^3E$ ($^3T_1$, P) | $^3A_2$ ($^3T_1$, P) | $^3E$ ($^3T_2$, F) | $^3A_1$ ($^3T_2$, F) | $^3E$ ($^3T_1$, F) |
|---|---|---|---|---|---|---|---|---|
| *Complex* | | | | | | | | |
| HB($^t$BuIm)$_3$NiBr (**3**) in $CD_2Cl_2$[b] | 36 400 (4500) | | 27 800 (500)[g] | 21 150 (210) | 14 490 (170, sh) | 13 530 (290) | Absent[h] | 7250, 8600 (170) |
| By AOM[c] | | | | | | | | |
| $\varepsilon_\pi(C) \equiv 0$ | | | 25 080 | 20 210 | 14 960 | 13 860 | 10 560 | 7690 |
| $\varepsilon_{\pi\text{-}s(y)}(C) \neq 0$ | | | 24 470 | 19 900 | 14 680 | 13 560 | 10 300 | 7590 |
| $\varepsilon_{\pi\text{-}c(x)}(C) \neq 0$ | | | 25 100 | 20 270 | 15 030 | 13 880 | 10 560 | 7720 |
| [Tp*Ni]Br in $CCl_4$[d] | 31 500 (2400) | 28 900 (640) | 20 220 (630) | 17 600 (90, sh) | 12 320 (160) | 11 110 (190) | Absent[h] | 6290 (60) |
| By AOM[c,e] | | | | | | | | |
| $\varepsilon_\pi(N) \equiv 0$ | | | 20 240 | 17 600 | 12 310 | 11 080 | 8030 | 6330 |
| $\varepsilon_{\pi\text{-}s(y)}(N) \neq 0$ | | | 20 220 | 17 580 | 12 310 | 11 060 | 8030 | 6320 |
| $\varepsilon_{\pi\text{-}c(x)}(N) \neq 0$[f] | | | 21 530 | 17 180 | 13 160 | 11 010 | 8750 | 5400 |

[a] Transitions from a $^3A_2(^3T_1, F)$ ground state.
[b] This work. $CD_2Cl_2$ was used for NIR spectra to eliminate $\nu$(CH) overtones.
[c] The LFT parameters are given in Table S1.
[d] Reported by Desrochers et al. for [Tp*]NiBr [30].
[e] Recalculated in this work, but based on Desrochers et al. [30].
[f] This fit, along among the four presented, was problematic in terms of parameter robustness as well as agreement with experiment.
[g] The transition $^3A_2(^3T_1, F) \rightarrow {}^3A_2(^3A_2, F)$ likely overlaps with LMCT and or ligand-based transitions.
[h] Forbidden in $C_{3v}$ symmetry. For **3**, there is a weak feature at ca. 11000 $cm^{-1}$ that may be due to this transition, which is allowed in lower symmetry.

experiment. We suspect that the ability to match exactly the experimental magnitude of $D$ with a satisfying choice of $\zeta$ may therefore be fortuitous. Unfortunately, we do not currently have available a chloro analog of **3**, so we cannot test the effectiveness of the calculation of zfs, as was successful for [Tp*]NiCl [30]. Heavy (i.e., $n > 2$) ligand atoms may have significant spin–orbit coupling contributions of their own (e.g., for free atom Br, $4p^5$, $\zeta = 2457\ cm^{-1}$ [55]; ~3.7 times that for free ion $Ni^{2+}$) which can greatly change the overall zfs, even to the extent of changing its direction to opposite from what would be expected based on a pure $d^n$ basis set. This has been convincingly demonstrated for a Mn(III) complex with iodo ligands [56]. That the bromo ligand plays a non-innocent role is clear from its large hyperfine coupling, as described above. Apparently, the electronic absorption spectrum of **3** can be modeled adequately using LFT with a $3d^8$ basis set, but more complicated (but lower energy), relativistic effects that give rise to hyperfine coupling and zfs cannot be treated so simply. For example, another complication is spin–spin coupling, which cannot be treated using LFT, but can be with the latest DFT methods [57].

Qualitatively, in **3** there is a significant contribution of a valence isomer that can be represented as $[Ni(I)–Br^{\cdot}]^+$, in addition to the conventional isomer, $[Ni(II)–Br^-]^+$. The situation is analogous to that proposed by Craft et al. for Ni as found in the ox1 form of the enzyme methyl coenzyme M reductase (MCR) [58]. In $MCR_{ox1}$, the Ni ion is equatorially coordinated by a macrocyclic ligand (the $F_{430}$ cofactor) and axially by a sulfur donor. The best description of $MCR_{ox1}$ is one that contains a dominant contribution from $[Ni(II)–(RS^{\cdot})]^+$ over the originally proposed $[Ni(III)–(RS^-)]^+$ valence isomer. Craft et al. thus used the representation {Ni–SR}$^9$ to describe the oxidation states in $MCR_{ox1}$ [58], as is now standard for metal nitrosyl complexes [59]. Thus, by analogy with Ni-thiyl in $MCR_{ox1}$ [58], as well as metal nitrosyls, we feel that it is instructive in **3** to use the formalism {NiBr}$^{10}$, where the superscript refers to the sum of the Ni(II) $3d^8$ electrons plus a bromide lone pair. We do not claim any quantitative analysis of Ni–Br bonding in **3**, but are simply indicating that the situation is more complex that would be expected for a typical Ni(II) halide. A more traditional case of this oxidation state ambiguity is treated next, in the nitrosyl complex, **4**.

### 3.7. Synthesis and characterization of HB($^t$BuIm)$_3$Ni(NO) (**4**)

Synthesis of **4** was achieved by reaction of *in situ* prepared **2** and $Ni(NO)Br(PPh_3)_2$ [9]. This method has been successfully used to prepare nickel nitrosyl complexes with other tripodal ligands [3,8]. A deep purple solid was isolated in 84% yield and was characterized as HB($^t$BuIm)$_3$Ni(NO) (**4**) by X-ray crystallography.

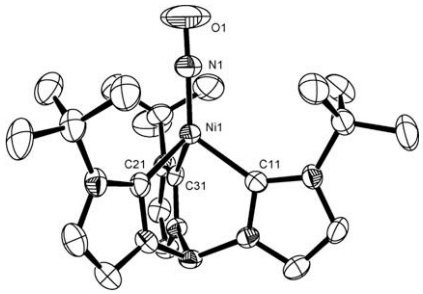


**Fig. 9.** ORTEP of HB($^t$BuIm)$_3$Ni(NO) (**4**) with hydrogen atoms removed for clarity. Thermal ellipsoids shown are at 50% probability.

The X-ray crystal structure of **4** confirms the monomeric, four-coordinate nickel complex (Fig. 9). The tris(carbene)borate ligand is coordinated to the nickel center in a tridentate fashion, similar to **3**. The Ni–C bond lengths (1.992(4)–2.017(6) Å), C–Ni–C bond angles (90.08(16)–92.0(3)°) and N–Ni–C bond angles (123.5(2)–125.9(2)°) of **4** are similar to those in **3**. The Ni–N bond of **4** is short (Ni–N bond length is 1.620(5) Å) and the nitrosyl ligand is linear (Ni–N–O bond angle is 178.5(4)°).

The $^1$H NMR spectrum of **4** is consistent with a diamagnetic species and with the X-ray crystal structure: four resonances are observed between 0 and 10 ppm. Two resonances at $\delta = 6.97$ and 6.65 ppm are assigned to the imidazol-2-ylidene groups, a resonance at $\delta = 4.5$ ppm to the BH group (which is very broad due to unresolved coupling to $^{10,11}$B), and one resonance indicative of the *tert*-butyl groups at $\delta = 1.68$ ppm. The presence of the nitrosyl group was confirmed by IR spectroscopy as a band at 1703 $cm^{-1}$ (toluene).

Complex **4** has an {NiNO}$^{10}$ configuration according to the Enemark–Feltham notation [59]. Mononitrosyl compounds containing linear M–N–O groups are usually assumed to contain bound $[NO]^+$ (0-electron π-donor), whereas those having bent M–N–O arrangements are regarded as containing $[NO]^-$ (2-electron π-donor; both types of nitrosyl are shown in Fig. 10a and b, respectively) [60]. This structural criterion rules out an oxidation state assignment

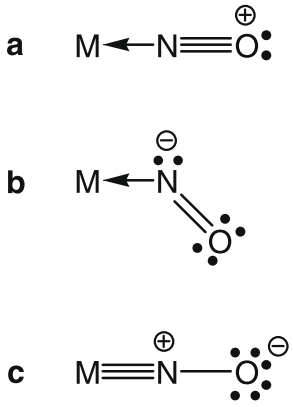


**Fig. 10.** Ionic representation of metal–nitrosyl bonding, showing formal charges on the nitrosyl ligand only (a) linear $[NO]^+$, (b) bent $[NO]^-$ and (c) linear $[NO]^{3-}$.

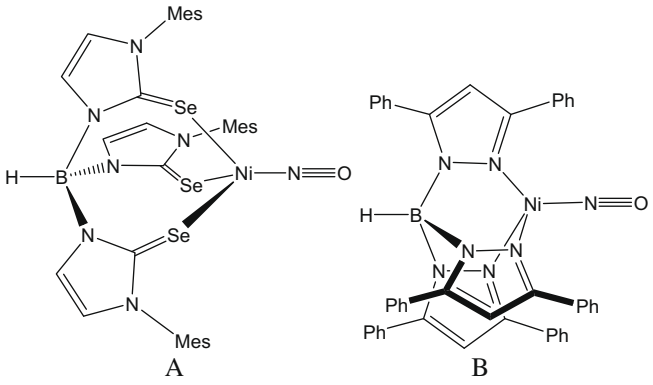


**Fig. 11.** Molecular structures of $[Tse^{Mes}]Ni(NO)$ (A) and $[Tp^*]Ni(NO)$ (B), where $Tse^{Mes}$ = tris(2-seleno-1-mesitylimidazolyl) hydroborate and $Tp^*$ = tris(3,5-dimethylpyrazolyl)hydroborate.

as Ni(II) ($3d^8$) with $NO^-$ for **4**. Furthermore, an assignment to Ni(II) would likely have $S = 1$, as seen for **3**, but not for **4**.

A problem with defining linear nitrosyl ligands as $[NO]^+$, however, is that unusual metal oxidation number assignments can result [61]. In the case of pseudo-tetrahedral nickel nitrosyl complexes, $\{NiNO\}^{10}$, such as in **4**, assignment of the linear nitrosyl ligand as $NO^+$ requires Ni(0). This assignment has been challenged by Parkin and co-workers [8]. On the basis of experimental and computational studies, they propose that the nitrosyl ligand in such complexes should be treated similarly to an trianionic nitride ($N^{3-}$), and thus isoelectronic to peroxide ($O_2^{2-}$) rather than to CO. This type of coordination is shown in Fig. 10c. Evidence for this proposal comes from the relatively short Ni–N(O) bond lengths found in $[Tp^*]NiNO$ and $[Tse^{Mes}]NiNO$ (1.634 and 1.618 Å, respectively) (Fig. 11), which are virtually identical to the Ni–N bond length calculated for the hypothetical compound $[Tp^*]Ni{\equiv}N$ (1.622 Å) [8]. Additionally, the $\nu$(NO) bands found for $[Tp^*]NiNO$ (1786 $cm^{-1}$) and $[Tse^{Mes}]NiNO$ (1763, 1752 $cm^{-1}$) are consistent with Ni–N $\pi^*$ back donation. By this argument, these nickel nitrosyl complexes would contain formally Ni(IV) and not Ni(0). Magnetic resonance does not aid in this distinction, except to confirm the diamagnetism, since each possibility contains two diamagnetic components: Ni(IV) (low-spin $3d^6$, $S = 0$) with $[NO]^{3-}$ versus Ni(0) ($3d^{10}$) with $NO^+$.

The experimental data for **4** leads us also to favor the $[NO]^{3-}$ oxidation state assignment. Specifically, the Ni–N bond length of **4** (1.620(5) Å) is the same as the Ni–N bond length in the hypothetical $[Tp^*]Ni{\equiv}N$ (1.622 Å). Furthermore, the relatively low $\nu$(NO) of **4** (1703 $cm^{-1}$) is consistent with a considerable amount of Ni–N $\pi^*$ back donation.

**Table 4**
$\nu$(NO) stretching frequencies of four-coordinate $\{NiNO\}^{10}$ complexes.

| Complex[a] | $\nu$(N–O) ($cm^{-1}$) | Reference |
|---|---|---|
| CpNi(NO) | 1839 | [10] |
| $[Tp^{Ph2}]Ni(NO)$ | 1803 | [4] |
| $Cp^*Ni(NO)$ | 1787 | [11] |
| $[Tp^*]Ni(NO)$ | 1786 | [8] |
| $[Tse^{Mes}]Ni(NO)$ | 1763, 1752 | [8] |
| $(PhS)_3Ni(NO)^{2-}$ | 1756[b] | [65] |
| $(Tm^{tBu})Ni(NO)$ | 1741 | [3] |
| $PhB(CH_2PPh_2)_3Ni(NO)$ | 1737 | [5] |
| $HB(^tBuIm)_3Ni(NO)$ | 1703 | This work |

[a] Cp = cyclopentadienyl, $Tp^{Ph_2}$ = tris(3,5-diphenylpyrazolyl)hydroborate, $Cp^*$ = $\eta^5$-$C_5Me_5^-$, pentamethylcyclopentadienyl, $Tp^*$ = tris(3,5-dimethylpyrazolyl)hydroborate, $Tse^{Mes}$ = tris(2-seleno-1-mesitylimidazolyl) hydroborate, $Tm^R$ = tris(mercaptoimidazolyl)hydroborate (R = Tol and $^t$Bu), and $PhB(PPh_2)_3^-$ = tris(phosphino)-phenylborate).

[b] Measured in $CH_3CN$; $\nu$(NO) = 1655 $cm^{-1}$ in the solid state.

### 3.8. Comparison of $\nu$(NO) with related complexes

The position of $\nu$(NO) in the IR spectrum can be used to evaluate the electron-donor ability of the tris(carbene)borate ligand. The position of $\nu$(NO) in **4** compared to a number of related nickel nitrosyl complexes (Table 4) shows that the $HB(^tBuIm)_3^-$ ligand is the most strongly electron donating among these.

To determine the influence of the tris(carbene)borate substituents on $\nu$(NO), three related complexes were prepared, namely $PhB(^tBuIm)_3Ni(NO)$, $PhB(MesIm)_3Ni(NO)$ and $PhB(MeIm)_3Ni(NO)$ (Table 4). These complexes were prepared as described above for **4** using the salt precursors: $PhB(^tBuImH)_3(OTf)_2$ [13], $PhB(MesImH)_3(OTf)_2$ [13] and $PhB(MeImH)_3(OTf)_2$ [18] and were characterized by $^1$H NMR, mass spectrometry (Section 2.3) and IR spectroscopy (Table 5).

Two observations regarding the position of $\nu$(NO) in these complexes can be made. The first is that there is no significant change in $\nu$(NO) when switching the group bound to boron from a hydrogen to a phenyl, suggesting that the boron atom is electronically isolated from the N-heterocyclic carbene donors. This is similar to observations made in diaryl bis(phosphino)borato platinum methyl carbonyl complexes $[R_2BPR'_2]Pt(Me)(CO)$ [62] where there

**Table 5**
Nitrosyl stretching frequencies of alkyl/aryl-substituted tris(carbene)borate $\{NiNO\}^{10}$ complexes.

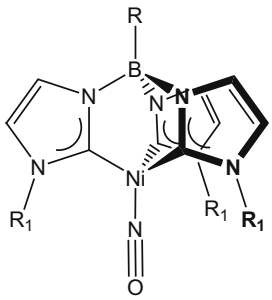


| R | $R_1$ | $\nu$(N–O) ($cm^{-1}$) |
|---|---|---|
| Ph | Mes | 1724 |
| H | $^t$Bu | 1703 |
| Ph | $^t$Bu | 1701 |
| Ph | Me | 1697 |

was no significant dependence of $\nu$(CO) on the nature of the *para* substituted phenyl groups.

The second observation concerns the effect of the imidazol-2-ylidene substituents, where the alkyl substituents have a lower $\nu$(NO) than the aryl substituent. The difference in stretching frequency shows that the alkyl substituted ligands are better electron donors than aryl substituted ligands. The greater electron-donor ability increases $\pi^*$ back donation from nickel to the nitrosyl ligand. The impact of the ligand substituents in these tris(carbene)borate ligands can be compared with results for unidentate N-heterocyclic carbene (NHC) ligands. In a series of unidentate NHC complexes, (NHC)Ir(CO)$_2$Cl (NHC = 1,3-substituted imidazol-2-ylidene) [63] alkyl substituted ligands had a greater donor ability than aryl substituted ligands, e.g., (IAd)Ir(CO)$_2$Cl $\nu$(CO) = 2063.4 cm$^{-1}$ versus (IPr)Ir(CO)$_2$Cl $\nu$(CO) = 2066.8 cm$^{-1}$ (IAd = 1,3-adamantylimidazol-2-ylidene, IPr = 1,3-(2,6-diisopropylphenyl)imidazol-2-ylidene). By contrast, no significant change in the electron donor capability of different NHC substituents was observed in (NHC)Ni(CO)$_3$ complexes [64].

## 4. Conclusions

In summary, the tris(carbene)borate complexes HB($^t$BuIm)$_3$NiBr (**3**) and HB($^t$BuIm)$_3$NiNO (**4**) have been prepared and fully characterized. In particular, HFEPR was used to investigate the $S = 1$ ground state of the bromide complex, **3**. Analysis of the electronic absorption spectra of **3** give evidence for the strong σ-donating ability of the tris(carbene)borate ligand. This ligand may also act as a π-acceptor. The significant hyperfine interaction observed from the bromo ligand and the difficulty in reproducing the sign of the zfs both suggest that this complex can be meaningfully represented as {NiBr}$^{10}$, by analogy with Ni nitrosyl and thiyl complexes, rather than simply as a classical Ni(II) bromide. The nickel nitrosyl complex, **4**, clearly fits into the classification as {NiNO}$^{10}$. The X-ray crystal structure and IR data of **4**, however, are consistent with the proposal of multiple bond character between Ni and N of the nitrosyl ligand. The position of $\nu$(NO) for tris(carbene)borate complexes is consistent with high electron-donor ability. That ability can be further tuned by changes to the substituents on the imidazol-2-ylidene moieties of the ligand, as was pioneered by Trofimenko for tris(pyrazolyl)borate ligands [2]. Future work will address metal–tris(carbene)borate ligand bonding in other four- and six-coordinate complexes as well as metal–ligand multiple bonds in complexes supported by tris(carbene)borate ligands.

## Acknowledgements

This work has been supported by the ACS-PRF (J.M.S.) and by the NHMFL (UGCP J.K. & J.T.), which is funded by NSF (Cooperative Agreement DMR 0654118), the State of Florida, and DOE. The 25-T magnet at NHMFL was funded by the W. M. Keck Foundation and the UV–Vis–NIR spectrophotometer at Roosevelt U. by the Goldenberg Foundation. I.N. is supported by the NIH (RISE GM 61222). The Bruker X8 X-ray diffractometer was purchased via an National Science Foundation CRIF:MU award to the University of New Mexico. We thank Eileen Duesler for X-ray data collection. Finally, we acknowledge Jerry Trofimenko's seminal contributions to inorganic chemistry that have helped inspire our research.

## Appendix A. Supplementary material

CCDC 602657 and 619042 contain the supplementary crystallographic data for **3** and **4**. These data can be obtained free of charge from The Cambridge Crystallographic Data Centre via http://www.ccdc.cam.ac.uk/data_request/cif. Supplementary data associated with this article can be found, in the online version, at doi:10.1016/j.ica.2009.05.015.

## References

[1] S. Trofimenko, Scorpionates: The Coordination Chemistry of Polypyrazolylborate Ligands, Imperial College Press, London, UK, 1999. p. 292.
[2] S. Trofimenko, Polyhedron 23 (2004) 197.
[3] L.S. Maffett, K.L. Gunter, K.A. Kreisel, G.P.A. Yap, D. Rabinovich, Polyhedron 26 (2007) 4758.
[4] D.J. Harding, P. Harding, H. Adams, T. Tuntulani, Inorg. Chim. Acta 360 (2007) 3335.
[5] C.E. MacBeth, J.C. Thomas, T.A. Betley, J.C. Peters, Inorg. Chem. 43 (2004) 4645.
[6] P.J. Schebler, C.G. Riordan, I.A. Guzei, A.L. Rheingold, Inorg. Chem. 37 (1998) 4754.
[7] K. Pang, J.M. Tanski, G. Parkin, Chem. Commun. (2008) 1008.
[8] V.K. Landry, K. Pang, S.M. Quan, G. Parkin, Dalton Trans. (2007) 820.
[9] R.D. Feltham, Inorg. Chem. 3 (1964) 116.
[10] O. Crichton, A.J. Rest, J. Chem. Soc., Dalton Trans. (1977) 986.
[11] J.C. Green, C. Underwood, J. Organomet. Chem. 528 (1997) 91.
[12] I. Nieto, F. Cervantes-Lee, J.M. Smith, Chem. Commun. (2005) 3811.
[13] R.E. Cowley, R.P. Bontchev, E.N. Duesler, J.M. Smith, Inorg. Chem. 45 (2006) 9771.
[14] R.E. Cowley, R.P. Bontchev, J. Sorrell, O. Sarracino, Y. Feng, H. Wang, J.M. Smith, J. Am. Chem. Soc. 129 (2007) 2424.
[15] I. Nieto, F. Ding, R.P. Bontchev, H. Wang, J.M. Smith, J. Am. Chem. Soc. 130 (2008) 2716.
[16] J.J. Scepaniak, M.D. Fulton, R.P. Bontchev, E.N. Duesler, M.L. Kirk, J.M. Smith, J. Am. Chem. Soc. 130 (2008) 10515.
[17] J.M. Smith, Comments on Inorganic Chemistry 29 (2008) 189.
[18] A.P. Forshaw, R.P. Bontchev, J.M. Smith, Inorg. Chem. 46 (2007) 3792.
[19] I. Nieto, R.P. Bontchev, J.M. Smith, Eur. J. Inorg. Chem. (2008) 2476.
[20] L.M. Venanzi, J. Chem. Soc. (1958) 719.
[21] S.A. Zvyagin, J. Krzystek, P.H.M. van Loosdrecht, G. Dhalenne, A. Revcolevschi, Physica B 346–347 (2004) 1.
[22] A.K. Hassan, L.A. Pardi, J. Krzystek, A. Sienkiewicz, P. Goy, M. Rohrer, L.-C. Brunel, J. Magn. Reson. 142 (2000) 300.
[23] M.V. Baker, L.D. Field, T.W. Hambley, Inorg. Chem. 27 (1988) 2872.
[24] J. Krzystek, S.A. Zvyagin, A. Ozarowski, S. Trofimenko, J. Telser, J. Magn. Reson. 178 (2006) 174.
[25] P. Kottis, R. Lefebvre, J. Chem. Phys. 41 (1964) 379.
[26] S.K. Smoukov, J. Telser, B.A. Bernat, C.L. Rife, R.N. Armstrong, B.M. Hoffman, J. Am. Chem. Soc. 124 (2002) 2318.
[27] B.N. Figgis, M.A. Hitchman, Ligand Field Theory and its Applications, Wiley-VCH, New York, 2000.
[28] J. Bendix, M. Brorson, C.E. Schäffer, Inorg. Chem. 32 (1993) 2838.
[29] T.R. Belderraín, M. Paneque, E. Carmona, E. Gutiérrez-Puebla, M.A. Monge, C. Ruiz-Valero, Inorg. Chem. 41 (2002) 425.
[30] P.J. Desrochers, J. Telser, S.A. Zvyagin, A. Ozarowski, J. Krzystek, D.A. Vicic, Inorg. Chem. 45 (2006) 8930.
[31] R.S. Drago, Physical Methods for Chemists, second ed., Saunders College Publishing, Ft. Worth, 1992.
[32] C. Benelli, I. Bertini, D. Gatteschi, J. Chem. Soc., Dalton Trans. (1972) 661.
[33] I. Bertini, C. Luchinat, Coord. Chem. Rev. 150 (1996) 1.
[34] P.J. van Dam, A.A.K. Klaassen, E.J. Reijerse, W.R. Hagen, J. Magn. Reson. 130 (1998) 140.
[35] P.L.W. Tregenna-Piggott, H. Weihe, J. Bendix, A.-L. Barra, H.-U. Güdel, Inorg. Chem. 38 (1999) 5928.
[36] I. Krivokapic, C. Noble, S. Klitgaard, P.L.W. Tregenna-Piggott, H. Weihe, A.-L. Barra, Angew. Chem., Int. Ed. 44 (2005) 3613.
[37] J. Martinez-Lillo, J. Faus, M. Julve, F. Lloret, S. Nellutla, J. Krzystek, NHMFL 2008 Research Report, Available on-line through: <http://www.magnet.fsu.edu/mediacenter/publications/reports/2008annualreport/2008-NHMFL-Report17.pdf>.
[38] A.C. Doyle, The Sign of Four, Spencer Blackett, London, 1890.
[39] P.W. Smith, R. Stoessiger, J. Chem. Soc. D (1971) 279.
[40] S. Takaishi, Y. Tobu, H. Kitagawa, A. Goto, T. Shimizu, T. Okubo, T. Mitani, R. Ikeda, J. Am. Chem. Soc. 126 (2004) 1614.
[41] M.J. Nilges, E.K. Barefield, R.L. Belford, P.H. Davis, J. Am. Chem. Soc. 99 (1977) 755.
[42] J.A. Weil, J.R. Bolton, J.E. Wertz, Electron Paramagnetic Resonance. Elementary Theory and Practical Applications, John Wiley & Sons Inc., New York, 1994.
[43] J. Krzystek, J.-H. Park, M.W. Meisel, M.A. Hitchman, H. Stratemeier, L.-C. Brunel, J. Telser, Inorg. Chem. 41 (2002) 4478.
[44] J.A. Larrabee, C.M. Alessi, E.T. Asiedu, J.O. Cook, K.R. Hoerning, L.J. Klingler, G.S. Okin, S.G. Santee, T.L. Volkert, J. Am. Chem. Soc. 119 (1997) 4182.
[45] T. Fujihara, T. Schönherr, S. Kaizaki, Inorg. Chim. Acta 249 (1996) 135.
[46] C.E. Schäffer, Struct. Bond. 5 (1968) 68.
[47] J.E. Davies, M. Gerloch, D.J. Phillips, J. Chem. Soc., Dalton Trans. (1979) 1836.
[48] M. Gerloch, L.R. Hanton, Inorg. Chem. 20 (1981) 1046.
[49] X. Hu, Y. Tang, P. Gantzel, K. Meyer, Organometallics 22 (2003) 612.
[50] D. Nemcsok, K. Wichmann, G. Frenking, Organometallics 23 (2004) 3640.

[51] L. Mercs, G. Labat, A. Neels, A. Ehlers, M. Albrecht, Organometallics 25 (2006) 5648.
[52] M.D. Sanderson, J.W. Kamplain, C.W. Bielawski, J. Am. Chem. Soc. 128 (2006) 16514.
[53] D.M. Khramov, V.M. Lynch, C.W. Bielawski, Organometallics 26 (2007) 6042.
[54] A. Bittermann, P. Härter, E. Herdtweck, S.D. Hoffmann, W.A. Herrmann, J. Organomet. Chem. 693 (2008) 2079.
[55] S. Fraga, G. Malli, Many-Electron Systems: Properties and Interactions, Saunders, Philadelphia, 1968.
[56] S. Mossin, H. Weihe, A.-L. Barra, J. Am. Chem. Soc. 124 (2002) 8764.
[57] D. Ganyushin, F. Neese, J. Chem. Phys. 125 (2006) 024103.
[58] J.L. Craft, Y.-C. Horng, S.W. Ragsdale, T.C. Brunold, J. Am. Chem. Soc. 126 (2004) 4068.
[59] J.H. Enemark, R.D. Feltham, Coord. Chem. Rev. 13 (1974) 339.
[60] J.A. McCleverty, Chem. Rev. 104 (2004) 403.
[61] G.B. Richter-Addo, P.B. Legzdins, Metal Nitrosyls, Oxford University Press, New York, 1992.
[62] J.C. Thomas, J.C. Peters, Inorg. Chem. 42 (2003) 5055.
[63] R.A. Kelly, H. Clavier, S. Giudice, N.M. Scott, E.D. Stevens, J. Bordner, I. Samardjiev, C.D. Hoff, L. Cavallo, S.P. Nolan, Organometallics 27 (2008) 202.
[64] R. Dorta, E.D. Stevens, N.M. Scott, C. Costabile, L. Cavallo, C.D. Hoff, S.P. Nolan, J. Am. Chem. Soc. 127 (2005) 2485.
[65] A.G. Tennyson, S. Dhar, S.J. Lippard, J. Am. Chem. Soc. 130 (2008) 15087.